ABUAD Journal of Engineering Research and Development (AJERD)
ISSN (online): 2645-2685; ISSN (print): 2756-6811

Volume 7, Issue 2, 308-316

Low and High Gas Tungsten Arc Welding Heat Inputs Influence on Corrosion of Stainless Steel Weldments

Bolarinwa Johnson KUTELU[1], Akinlabi OYETUNJI[2], Daniel Toyin OLORUNTOBA[2]

[1]*Department of Mineral and Petroleum Resources Engineering Technology, The Federal Polytechnic Ado-Ekiti, Ekiti, State, Nigeria*
rinwa2006@yahoo.com

[2]*Department of Metallurgical and Materials Engineering, Federal University of Technology, Akure, Ondo State, Nigeria*
aoyetunji@futa.edu.ng/dtoloruntoba@futa.edu.ng

Corresponding Author: rinwa2006@yahoo.com, +2347033436658
Date Submitted: 19/07/2024
Date Accepted: 09/09/2024
Date Published: 15/09/2024

Abstract: *In this study, influence of low and high heat inputs on corrosion susceptibility of 304L austenitic stainless steel (ASS) in simulated 0.5 molar solution of NaCl was investigated. Gas tungsten arc welding (GTAW) was used to generate low and high levels welding heat input. Microstructures of the weldments were examined, using metallurgical optical microscope (OMM) (Olympus GX51), while the corrosion behaviours were evaluated by potentiodynamic polarization tests, and corrosion data were recorded, using a computer-based data logging system – Autolab PGSTAT 204N. From the results, the evolving microstructures of the weldments before corrosion were characteristically heterogeneous; austenite (γ) was the leading phase, while ferrite (α) grains were dispersed within the γ matrix. Fusion zone (FZ) and heat affected zone (HAZ) microstructures after corrosion were characterised by pits of varying sizes with different alignments. And at GTAW speed, current and voltage of 7.2 mm/s, 200A and 40V, corresponding to low heat inputs, there were few number and size of pits relative to 1.7 mm/s, 200A and 40V, corresponding to high heat input. Shift in corrosion potentials (E_{corr}) toward less negative direction, that is more nobility was observed at the low heat inputs induced GTAW parameters as compared to the corresponding high heat inputs induced GTAW parameters. In general, corrosion susceptibility of 304L ASS in the simulated 0.5 molar solution of NaCl was heightened at high heat inputs induced GTAW parameters as compared to the corresponding low heat inputs parameters.*

Keywords: *Corrosion, 304L Austenitic Stainless Steel, Weldments, Microstructures, Chloride Environment*

1. INTRODUCTION

Welding is a process of materials joining, which involves coalescing of two or more parts at their contacting surfaces by the application of heat and/or pressure. Some materials can be welded by heat alone, with no pressure applied, while some by pressure alone, with no external heat supplied, and others may involve a combination of both heat and pressure [1,2]. 304L ASS is characterised by good weldability, making accomplishment of its maintenance and/or repairs be majorly by heat alone. As a result, arc welding processes, which are characterised by heat intensiveness [shielded metal arc welding (SAW), submerged arc welding (SMAW), plasma arc welding (PAW) and gas tungsten arc welding (GTAW)] have been successfully used to produce 304L ASS weldments [3,4,5,29].

GTAW is a choice welding technique in a number of industries such as oil and petrochemical fields, chemical plants, biomedical implants and food where its application is required, however composition and microstructural features of weldments, and hence weld quality differ considerably from the base metal [5,6,23, 32]. For instance, small δ–ferrite of varied amount, which featured in the final microstructure of 316L ASS, which was maintained by GTAW process, was attributed to incomplete transformation of δ to γ that resulted from effect of welding heat input [6, 32]. Average γ and α grains in HAZ, equiaxed fine γ and α grains in FZ and varied amount of columnar weld metal in bulk of deposit of stainless steel weldments were attributed to influence of welding heat input [6]. Reduction in load-carrying capacity of the connection between quenched and tempered steel weldments, which resulted from softening of material adjacent to the weld was attributed to high heat input [16, 8]. Low hardness along large weld zone of HAZ, which resulted from long dendrites and large interdendritic was due to high heat input. While high hardness along small weld zone of HAZ, which resulted from short dendrites and small interdendritic spacing was due to low heat input [8,6]. Increase in mechanical properties of ASS weldment, which was due to increased presence of dendritic structures was related to high welding heat input, and decrease in mechanical properties of ASS weldment, which was due to decreased presence of dendritic

structures was related to low welding heat [8, 14, 49]. Achebo, [9] attributed reduction in performance integrity of the weldment, which was produced at high heat input to loss of alloying elements at the weld pool. Kozuh et al. [7] attributed increase in pitting corrosion to large cathode areas that resulted at high heat input. Precipitates and inclusions in stainless steels microstructures are sites for pit initiation, and their presence in microstructures are significantly influenced by welding heat input [7,10,28, 44].

Mohd et al. [11] investigated influence of welding parameters on mechanical properties of underwater welded mild steel specimen (C, Mn, Si) with insulated electrode E6013. They revealed that with increased welding speed at constant voltage and current, quality of weld metal and mechanical properties (ultimate tensile strength (UTS), hardness (BHN) and impact strength) were increased until optimum ultimate tensile strength (UTS), hardness (BHN) and impact strength were reached, after which further increase resulted in decreased ultimate tensile strength (UTS), hardness (BHN) and impact strength. Ahmed et al. [12] investigated the effect of TIG welding speed on tensile strength of mild steel plate with 5 mm thickness, and reported that the UTS of the weld zone (WZ) was less as compared to the base metal (BM), the UTS increased as welding speed was decreased.

The welding heat input depends on welding parameters, including speed, current, voltage [36, 43], it therefore implies that proper choice of welding parameters, is critical for achieving the desired weld joints qualities. Consequently, in this study, welding heat input at high and low levels were introduced into 304L ASS through appropriate choice of GTAW parameters (speed, current and voltage). This is with the objective of assessing their effects on weld joint characteristics and, in consequence, corrosion susceptibility.

2. RELATED WORK

Heat input is a relative measure of the energy transferred per unit length of weld, and in arc welding, for instance, heat input plays an essential factor in quality control, welding heat input produces temperature gradient in the base metal [1,10,13, 22,38]. Ghusoon et al. [1] have shown that cooling rate is slow at high heat input and fast at low heat input, and that slow welding speed ensures more residence time of electrode on the workpiece, leading to long dendritic growth and inter dendritic spacing. From the plot of temperature against time (Figure 1), higher heat input slows slower cooling rate and lower heat shows faster cooling rate. The expression in equation 1 can be used to obtain heat input amount at any welding speed, current and voltage [1].

$$Q = {}^{\eta VI}/_{S} \quad (1)$$

Where;

Q is heat input (J/mm),
η is efficiency factor of the arc (For GTAW, η is 0.6),
V is arc voltage (V).
I is welding current (A) and
S is welding speed (mm/s).

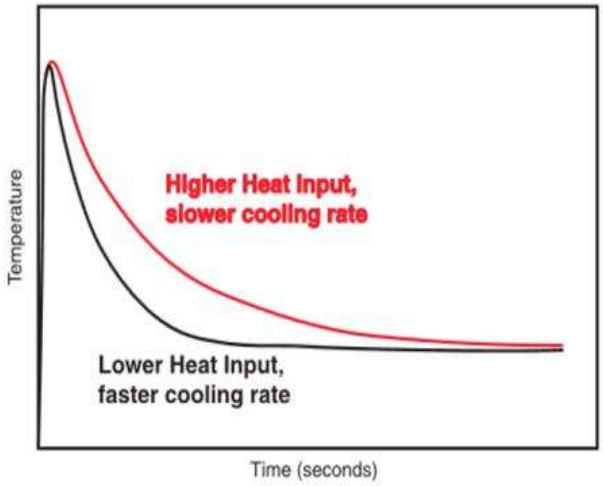

Figure 1: Effect of welding heat input on cooling rate [1]

Wan Shaiful et al. [14] investigated effect of welding heat input on microstructure and mechanical properties at coarse grain heat affected zone (CGHAZ) of ABS grade A. Flux cored arc welding (FCAW) technique was used, and the weldments were produced at low heat (0.99 kJ/mm), medium heat (1.22 kJ/mm) and high heat (2.25 kJ/mm). From their report, microstructure of the CGHAZ was consisted of grain boundary ferrite (GBF), Widmanstatten ferrite (WF) and pearlite (P). And significant grain coarsening occurred at the CGHAZ of all the joints, extent of grain coarsening was

increased with increasing heat input. The joints made at low heat input exhibited high hardness and impact toughness value relative to medium and high heat input respectively. It was concluded that at high heat input, grain growth occurred with concomitant reduction in hardness and toughness properties. Tabish et al. [15] studied effect of heat input on microstructure and mechanical properties of TIG welded joints of AISI 304 SS, and reported that microstructure was characterised by large dendrites at high heat input as compared to medium and low heat inputs respectively. And the weldment showed high tensile strength at low heat input and low tensile strength at high heat input.

Oyetunji et al. [5] investigated influence of varied metal arc welding (GTAW) speed and power input on microstructural characteristics and tensile behaviour of type 304L austenitic stainless steel (ASS) heat affected zone (HAZ), and their report, microstructures were consisted of mixture of austenite and ferrite phases with varied volume fraction and grain size. Chromium carbide formation and precipitation were apparent at grain boundaries. Optimum ultimate tensile strength (UTS) and yield strength (YS) were obtained for HAZ sample at moderate welding speed, while optimum % elongation was obtained at slow welding speed. Optimum UTS and YS were obtained for HAZ sample at power input of 9.2 KW, while optimum % elongation was obtained at power input of12.00 KW. Kožuh et al. [6] investigated mechanical properties and microstructure of 316 ASS after welding and post-weld heat treatment, and reported that low ferrite number was as a result of high concentrations of C, Mn, Ni, and N. The fully austenitic microstructure revealed increased propensity for crack formation relative to the microstructure, which was comprised of austenite with a small amount of ferrite.

Amer et al. [3] investigated influence of welding parameters variation on the weldability of ASSl 304L. They attributed dendrites of varied sizes and numbers across the weldments to heat input and the resulting cooling rates. Laura et al. [16] investigated corrosion behavior of austenitic stainless steel welds that was prepared by dual protection GTAW process in 0.5 M H2SO4 and 3.5%wt. NaCl. Increase in weld penetration was reported, which they attributed to oxygen that was incorporated into the weld pool. Increase in penetration-to-width ratio of approximately 3 times compared to the conventional GTAW setup with pure Ar shielding gas was attributed to employment of a 2.5% CO_2 concentration on the outer gas layer. Welds produced with 2.5% CO_2 dual shielding showed similar microstructure as weld produced by conventional GTAW process, addition of CO_2 led to small increases in corrosion rate in acid media, this however did not alter the uniform and pitting corrosion resistance in 3.5%NaCl aqueous solution.

Bakour et al. [17] studied effect of welding on corrosion resistance of austenitic stainless steel Alloy 59 (UNS N06027) and galvanic corrosion generated by the base/weld. The materials were exposed to polluted phosphoric acid at several temperatures; microstructures were studied by SEM and EDX analysis. And from their report, corrosion potential values to more anodic potentials. The corrosion current densities and the passive current densities were also observed to increase with increasing temperature. Kožuh et al. [7] analysed corrosion failure and microstructure of AISI 316L SSs for ship pipeline before and after welding, and attributed increased pitting to large cathode areas that resulted at high heat input. Shin et al. [18] studied the effects of heat input on pitting corrosion of super duplex stainless steel (SDSS), and reported that increase in cathodic area with time was initiated by precipitates. And that the pits that were initiated at the austenite-ferrite interfaces propagated into small cracks by coalescing and joining together with other neighbouring pits.

It is well known that 304LASS is characterized by excellent corrosion resistance, and it is commonly maintained and/or repaired by the GTAW technique, especially in applications, requiring to be operated in corrosive environment(s) [5,6,19,20,21]. However, research efforts on corrosion susceptibility of GTAW maintained/or repaired 304L ASS weldment has not been well reported in literatures. This is in spite of the considerable efforts that the past researchers have made in relating welding heat input to microstructure characteristics, mechanical properties and corrosion resistance (integrity performance) of the weld joint.

3. MATERIAL AND METHODS

3.1 Material

304L ASS pipe of 10 mm x 10 mm x 4.5 mm used for the investigation was obtained from Nigerian Foundries Limited, Ikorodu, Lagos State, Nigeria. Chemical compositions of the 304L ASS and filler rod employed are depicted in Tables 1 and 2 respectively.

Table 1: Chemical of the 304L ASS steel

C	0.026	Cl	0.002
Si	0.511	Mo	0.069
Mn	1.311	V	0.083
S	<0.001	Ti	0.036
P	0.013	Fe	75.916
Cr	18.325		
Ni	8.469		
Cu	0.135		
Nb	0.009		
Al	0.018		

Table 2: Chemical composition of the filler metal

Element	(Wt. %)
C	<0.03
Si	0.65
Mn	1.65
S	0.03
P	0.03
Cr	19.5-22.0
Ni	9.0-11.0

3.2 Methods

Samples with dimensions 50 mm x 30 mm x 4.5 mm were cut from the as-received 304L ASS pipe, using simple handsaw, and cleaned with acetone to remove lubricant and surface contamination [23] The samples were then machined to butt-joint specimens with weld configuration of single-V groove of 60° and root gap of 2.5 mm, which was necessary to ensure good root penetration [22,]. A manually operated Clark GTAW welding machine and stainless steel filler electrode with 2.5 mm diameter were used to produce the weldments at varied ranges of GTAW speed, current and voltage. Values of current and voltage were read directly from the GTAW machine, while values of speed were obtained by calculation using the expression in equation 2 [24]

$$S = {}^{L}/_{T} \quad (2)$$

Where;

S is welding speed (mm/s),

L is length (mm) and T is time (s). The time taken to produce each weldment was determined using a stop watch. The weldments were visually inspected for weld defects. Summary of the weldment production procedure is depicted in Table 3.

Table 3: Procedure for weldments production

S/No	Welding parameters		
1.	Speed (mm/s)	Current (A)	Voltage (V)
	1.7	160	30
	7.2	160	30
2.	Current(A)	Speed(mm/s)	Voltage (V)
	120	4.6	30
	200	4.6	30
3.	Voltage (V)	Current (A)	Speed (mm/s)
	20	160	30
	40	160	30

3.3 Metallography

Standard metallographic specimens with dimensions 50 mm length, 30 mm breadth and 4.5 mm thickness were cut and polished to a mirror-like surface by grinding, using silicon carbide paper of different mesh sizes (120, 240, 320, 400, 600, 800 and 1200) and subsequent grinding on emery cloth, using a suspension of alumina powder. The specimens were prepared in accordance with ASTM E3-11[25]. Thereafter, the specimens were etched in solution of 50 ml HCl + 50 ml HNO3 + 50 ml water for two minutes. After which, optical microscopy observation was made, using Olympus metallurgical microscope, model-GX51 with camera attached.

3.4 Electrochemical Studies

Corrosion coupons of dimension 20 mm x 10 mm x 4.5 mm were cut from the weldments and mounted in resin. The coupons were connected with a flexible wire, ground, polished, cleaned and rinsed properly following ASTM G36 standard [24]. The electrochemical studies were done, using a conventional three-electrode cell system, comprising saturated silver/silver chloride, platinum and the coupon (304LASS weldments) as reference electrode, counter/ auxiliary electrode and working electrode respectively. The experiments were performed at room (25^{o}C) temperature based on ASTM G5-94 [25]. Data were recorded, using a computer-based data logging system (Autolab PGSTAT 204N) piloted, which was by NOVA software. For the purposes of reliability and reproducibility, the experiments were reaped more than three times [7,26].

4. RESULTS AND DISCUSSION

4.1 Heat inputs

High heat input induced GTAW parameters (speed of 1.7 mm/s, current of 200A and voltage of 40V) and low heat input induced GTAW parameters (7.2 mm/s, 120 A and 20 V) shown in Table 4 were due to slow and fast cooling conditions respectively, which may be hinged on effects residence time of electrode on work piece [7].

Table 4: Heat input values of the weldment at the varied range of GTAW parameters

S/No.	Welding parameters			Heat input	
				Low	High
1.	Speed (mm/s)	Current(A)	Voltage (V)	J/mm	J/mm
	1.7	160	30		1694.5
	7.2	160	30	400.00	
2.	Current (A)	Speed (mm/s)	Voltage (V)		
	120	4.6	30	469.57	
	200	4.6	30		782.61
3.	Voltage(V)	Current (A)	Speed (mm/s)		
	20	160	4.6	417.39	
	40	160	4.6		834.78

4.2 Pre Corrosion Microstructures of the Weldments

Figure 2 (a and b; c and d; and e and f) are the pre-corrosion optical micrographs of the weldment at GTAW speed, current and voltage of 1.7 mm/s and 7.2 mm/s, 120 A and 200 A, and 20 V and 40 V respectively. The evolving microstructures are heterogonous, γ is the leading phase and α grain is dispersed within the γ matrix, and there is apparent variations in average grain size of γ and α exist across the fusion zone (FZ) and heat affected zone (HAZ) microstructures. Also, microstructures of FZ and HAZ are characterised by fine and coarse grains respectively. And varied number and size of δ-ferrite, precipitations, inclusions and dendrites are seen within FZ and HAZ microstructures. The microstructural heterogeneity (non- equilibrium microstructures) of the weldments may be attributed to temperature gradients that resulted during the GTAW process. Kožuh et al. [7] have related decrease in subsequent cooling rates that occurred during weld solidification to increase in distance from the fusion boundary. Also, the microstructural heterogeneity was aided by the resulting generated chemical gradients during the GTAW process [5,6,7].

Increased presence of interspersing ferrite in austenite matrix at high heat inputs (1.7 mm/s, 200A and 40V), depicted in Plates were due to the resulting slow cooling conditions [5,13,40, 43]. Also, long dendrites and wide inter-dendritic spacing, characterizing the microstructures at these ranges of parameters are attributable to slow cooling conditions as well [13,40]. The increased number of inclusions within the microstructures at 200A and 40 V may have resulted from chemical reactions between dissolved metallic elements such as Fe, Mn, Al, Si and Cr and non- metallic elements such as S and C [31]. Also, the inclusions may be due to possible oxidation at the weld pool surface [30,31].

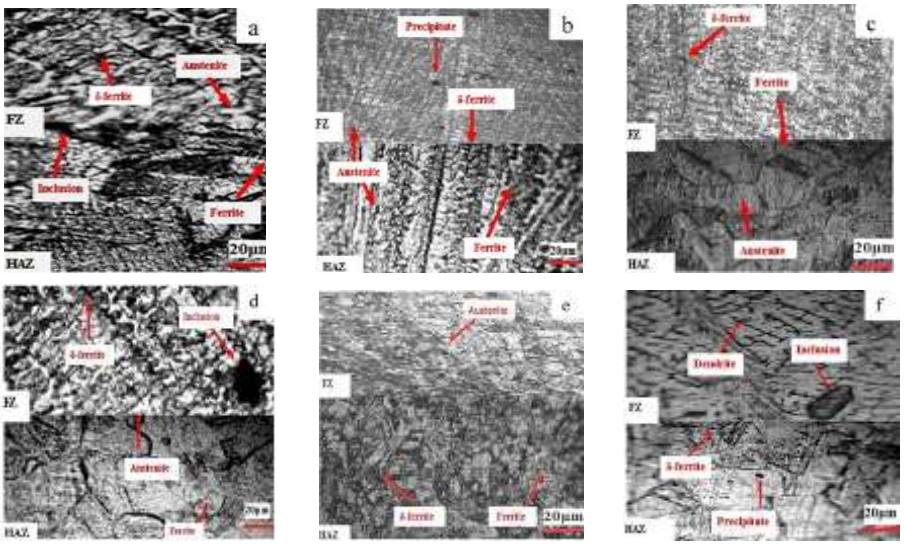

Figure 2(a-f). Pre -corrosion optical micrographs of the weldments at varied speed of 1.7 mm/s and 7.2 mm/s, current of 120 A and 200 A, and voltage of 20 V and 40 V respectively.

4.3 Corrosion Behaviour

The shift in corrosion potentials (Ecorr) toward less negative direction at 7.2 mm/s, 120 A and 20 V (i.e. more nobility) relative to 1.7 mm/s, 200 A and 40 V (i.e. less nobility), depicted in Figure 2a-c was due high dislocation density that resulted from low heat input, or fast cooling conditions. During which, more diffusion paths were provided for the migration of chromium to the surface, where homogeneous chromium-rich double layer corrosion products (Fe2O3 and Cr2O 3) passive film was formed [33, 34, 41, 46]. Saifu et al. [35] described electrochemical process of chromium oxide formation, using by equations. 3, 4 and 5. The chromium may possibly have existed as CrOOH and Cr (OH)3. These forms of oxides may have been converted to Cr2O3 by dehydration reaction to form a continuous dense film at the interface between reactions (34,42).

$$3FeO + 2Cr \rightarrow Cr_2O_3 + 3Fe \quad (3)$$

$$Cr3+ + 3OH- \rightarrow Cr(OH)_3 \quad (4)$$

$$Cr(OH)_3 + Cr + 3OH- \rightarrow Cr_2O_3 + 3H_2O + 3e-. Cr_2O_3 \quad (5)$$

The more nobility at 7.2 mm/s, 120 A and 20 V and less nobility at 1.7 mm/s, 200 A and 40 V (refer to Figure 3(a-c) resulted from high and low electrochemical stability of the formed surface oxide films respectively. In general, surface oxide films on fine-grained microstructure are characteristically compact, impervious and homogeneous, while those on coarse-grained microstructures are loose, pervious and inhomogeneous [33,35, 36, 43,45]. In addition, surface oxide breakdown has been related to grain size. Consequently, increased and decreased surface oxide break down was associated with coarse and fine grains respectively [34, 36]. Also, the less nobility (high susceptibility to corrosion attack) at high heat inputs was be due to weak spots in the passive film that resulted from inclusion, leading to direct exposure of boundaries between the inclusions and matrix to corrosive environment [39,44,45].

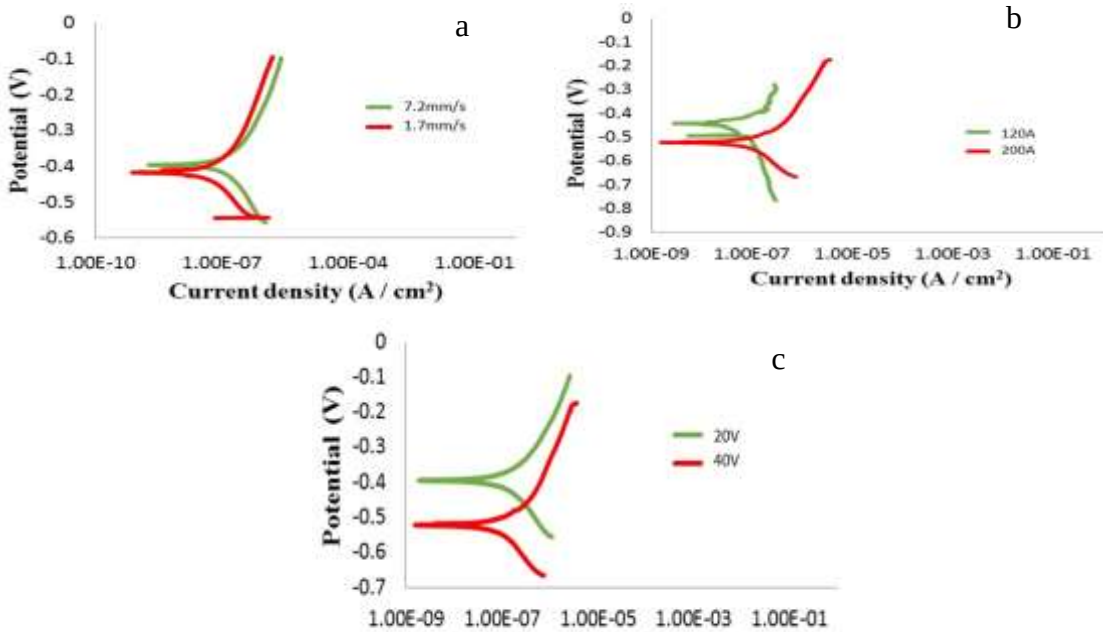

Figure 3(a- c). Potentiodynamic polarisation curves of the weldment at high and low GTAW speed, current and voltage respectively.

4.4 Post Corrosion Microstructure of the Weldments

FZs and HAZs post corrosion microstructures of the weldment at 25^{o}C are depicted in Figure 4 (g and h, i and j, and k and l). Characterising the microstructures, are pits, inclusions, precipitates and δ ferrite of varying sizes and alignment. The few number and size of pits at 7.2 mm/s, 120 A and 20 V relative to 1.7 mm/s, 200 A and 40 V was due to more volume fraction of austenite [36]. Characteristically, fine-grained microstructure has high boundary density, and grain boundary is more active than the bulk [37,43]. Therefore, it was expected that corrosion rate of fine-grained microstructure should be high relative to coarse-grained microstructure. And the observed departure from established principle may be hinged on palpable large cathode and small anode area combination [37,38]. The presence of more pits at 1.7 mm/s, 200 A and 40 V, corresponding to high heat input induced GTAW parameters as compared 7.2 mm/s, 120 A and 20 V corresponding to low heat input induced GTAW parameters was due to increased presence of δ-ferrite and inclusion, which are pit promoters, they acted as anode or cathode versus the alloy [47,48] or created boundaries with the matrix [45].

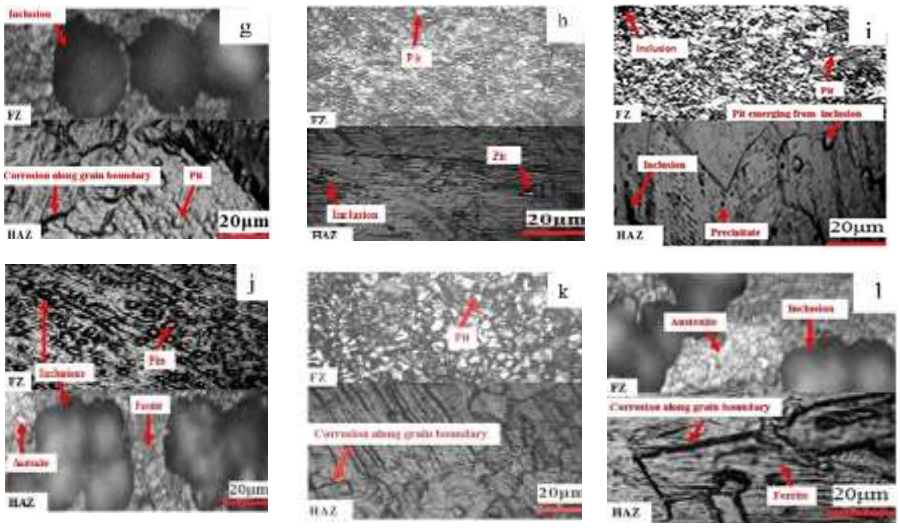

Figure 4 (g - l). Post - corrosion optical micrographs of the weldments at varied speed of 1.7 mm/s and 7.2 mm/s, current of 120 A and 200 A, and voltage of 20 V and 40 V respectively.

5. CONCLUSION

From the results of the investigation, the evolving microstructures of the weldments before corrosion were heterogeneous. Austenite (γ) is the leading phase, and ferrite (α) grains were dispersed within the γ matrix. Microstructures of the FZ and HAZ after corrosion were characterised by pits of varying sizes and different alignments. Inclusions, precipitates and δ - ferrite were obvious within the microstructures. The weldments produced at 7.2 mm/s, 120 A and 20 V revealed a few number and size of pits relative to those produced at 1.7 mm/s, 200A and 40V. And there was a shift in corrosion potentials (Ecorr) toward less negative direction that is more nobility at 7.2 mm/s, 120 A and 20 V as compared to 1.7 mm/s, 200 A and 40 V correspondingly. In general, corrosion susceptibility of the experimental 304L ASS weldments in the 0.5M simulated chloride environment was aggravated at the range of GTAW parameters that favour high heat input. This is in converse to the GTAW parameters that favour low heat input.

REFERENCES

[1] Ghusoon, R. M., Mahadzir, I., Syarifah, N. A. & Hassan A. A. (2017). Effects of Heat Input on Microstructure, Corrosion and Mechanical Characteristics of Welded Austenitic and Duplex Stainless Steels, A Review, Metals, 7 (39), 123-136.

[2] Lancaster, J. F. (2003). Metallurgy of welding, Chapman and Hale, London, 106-116.

[3] Amer, S. M., Morsy, M. A., Hussein. M. .A., Atlam, A. & Mosa E. S. (2015). Effect of Welding Parameters Variation on the Weldability of Austenitic Stainless Steel 304L. *International Journal of Scientific and Engineering Research*, 6 (2), 589-595.

[3] John, C. L. & Damian, J. K. (2005). Welding Metallurgy and Weldability of Stainless Steels, John Willey and Sons Inc. Hoboken, New Jersey, 30-32.

[4] Oyetunji, O., Kutelu, B. J. & Akinola, A. S. (2013). Effects of Welding Speeds and Power Inputs on the Hardness Property of Type 304L Austenitic Stainless Steel Heat-Affected Zone (HAZ). *Journal of Metallurgical Engineering (ME)*, 2(1), 124-129

[5] Kožuh, S., Goji´c. M. & Kosec., L. (2009). Mechanical Properties and Microstructure of Austenitic Stainless Steel after Welding and Post-Weld Heat Treatment, Kovove Mater. 47, 253–262.

[6] Kožuh, S. M.. Goji´c, M., Vrsalovi´c, L. & Ivkovi´c, B. (2013). Corrosion Failure and Microstructure Analysis of AISI 316l Stainless Steels for Ship Pipeline before and after Welding, Kovove Mater. 51, 53–61.

[7] Raveendra, S. (2012). Weldability and Process Parameter Optimization of Dissimilar Pipe Joints Using GTAW, *International Journal Eng., Res., Appl.*, 2, 2525-2530

[8] Achebo, J. I. (2012). Influence of Alloying Elements on HAZ Toughness of Multilayer Welded Steel Joints. *International Journal of Advances in Science and Technology*, 3 (4), 78 - 83.

[9] Apurv, C. & Vijaykumar, S. J. (2014). Influence of Heat Input on Mechanical Properties and Microstructure of Austenitic 202 Grade Stainless Steel Weldments, WSEAS Transactions on Applied and Theoretical Mechanics, 9, 222-228.

[10] Mohd, S., Mohd, F. & Hasan, P.K.B. (2014). Effect of Welding Speed, Current and Voltage on Mechanical Properties of Underwater Welded Mild Steel Specimen (C, Mn, Si) With Insulated Electrode E6013, MIT. *International Journal of Mechanical Engineering*, 4 (2), 120-124.

[11] Ahmed, K. H., Abdul, L., Mohd, J. & Pramesh T. (2010). Influence of Welding Speed on Tensile Strength of Welded Joint in TIG Welding Process. *International Journal of Applied Engineering Research, Dindigul*,. 1 (3), 518-527.
[12] Çalik, A. (2009). Effect of Cooling Rate on Hardness and Microstructure of AISI 1020, AISI 1040 and AISI 1060 Steels. *Int. J. of Phys. Sci*, 4 (9), 514-518.
[13] Wan Shaiful, H. W., Muda1, N. M. & Saifulnizan, J. (2015). Effect of Welding Heat Input on Microstructure and Mechanical Properties at Coarse Grain Heat Affected Zone of ABS Grade A steel. *ARPN Journal of Engineering and Applied Sciences*, 10 (20), 9487-9495.
[14] Tabish, T. A., Abbas T., Farhan, M., Atiq, S. & Butt, T. Z. (2014). Effect of Heat Input on Microstructure and Mechanical Properties of the TIG welded joints of AISI 304 Stainless Steel. *International Journal of Scientific and Engineering Research*, 5 , 2014 – 1532.
[15] Laura, L., Leonel, D., Abreu, C., Brasil, M. & Pedro, B. (2019). Corrosion Behaviour of Austenitic Stainless Steel Welds Prepared by Dual Protection GTAW Process in 0.5 M H2SO4 and 3.5%wt. NaCl. *Int. J. Electrochem. Sci*.,14, 1007-10092, www.electrochemsci.org
[16] Bakour S., Guenbour. A., Bellaouchou. A., Escrivà-Cerdán, C., Sánchez-Tovar R Leiva-García, R. & García- Antón, J. (2012). Effect of Welding on Corrosion Behaviour of a Highly Alloyed Austenitic Stainless Steel UNS N06027 in Polluted Phosphoric Acid Media. *International Journal of Electrochemical Science*, 7, 10530-10543.
[17] Shin, Y. T., Shin, H. S. & Lee H. W. (2012). Effects of Heat Input on Pitting Corrosion in Super Duplex Stainless Steel Weld Metals. Met. Mater. Int., 18, 1037–1040.
[18] Gopinath. S, Kuppusamy M.V & Ningshen. S. (2019). Corrosion Resistance Behavior of GTAW Welded AISI type 304L Stainless Steel, Trans India Inst. Met, 2981-2995, https://doi.org/10.1007/s12666-019-01779-w.
[19] Li. L, Dong C.F Xiao. K, Yao J.S. & Li X.G (2014). Effect of pH on Pitting Corrosion of Stainless Steel Welds in Alkaline Salt Water, Construction and Building Materials, 68, 708-715
[20] Kun-Chao T. & Chu-Ping Y (2022). The Corrosion Susceptibility of 304L Stainless Steel Exposed to Crevice Environments, Materials, 13, 3055.
[21] Subodh Kumar, Shashi A. S. & Dikshant Malhotra (2021). Effect of Welding Heat Input and Post-Weld Thermal Aging on the Sensitization and Pitting Corrosion Behaviour of AISI 304L Stainless Steel Butt Welds. *Journal of Materials Engineering and Performance*, 30, 1619-1640.
[22] Lawrence, O. O., Raheem, A. E. & Ikenna, C. E. (2016). Influence of Delta Ferrite on Corrosion Susceptibility of AISI 304 Austenitic Stainless Steel. *Materials Engineering Research Article*, 9, 120-128.
[23] Abioye T. E. (2017). Effect of Heat Input on the Mechanical and Corrosion Properties of AISI 304 Electric Arc Weldments. *British Journal of Applied Science and Technology*, 20(1), 1-10
[24] American Standard for Testing and Measurement E3-11 (2011). Standard guide for preparation of metallographic specimens, ASTM International, West Conshohocken
[25] American Standard for Testing and Measurement G36 (2014). Standard Guide for Preparation of Corrosion coupons, ASTM International, West Conshohocken
[26] American Standard for Testing and Measurement G5 – 94 (2004). Standard Reference Test Method for Making Potentiostatic and Potentiodynamic Anodic Polarization Measurements
[27] Saefuloh, I., Kanani, N., Gumelar. Ramadhan F., Rukmayyadi, Y., Yusuf, Y., Syarif, A. & Sidik, S. (2020). The Study of Corrosion Behaviour and Hardness of AISI Stainless Steel 304 in Concentration of Chloride Acid Solution and Temperature Variations. *Journal of Physics, Conference Series*, 1477
[28] Kutelu B. J., Adubi E. G. & Seidu S. O. (2018). Effects of Electrode types on the Microstructure, Tensile and Hardness Properties of 304 L *austenitic stainless steel heat-affected zone* (HAZ). *Journal of Minerals and Materials Characterization and Engineering*, 6, 32-38.
[29] Francisco-Javier C., Manuel Pascuel-Guillamon L.S.G., Fidel S.V., & Miguel-Angel P. (2019). Pitting corrosion of AISI 304 rolled stainless steel welding at different deformation levels. *Journal of Applied Sciences*, 9(16), 3265
[30] Woods R. A. & Milner D. R. (1971). Motion in the Weld Pool in Arc Welding, *Welding Journal*, 50 (4), 163-173.
[31] Arpita, N. B. & Vikram, A. P. (2016). Influence of Process Parameters of TIG Welding Process on Mechanical Properties of 304LSS Welded Joint, International Research Journal of Engineering and Technology, 3, 977.
[32] Xiancyan, Z.H.A.O., Xiwu, L.I.U., Xin, C.U.I., & Fengchang, Y. (2018). Corrosion Behavior of 304L in Nitric Acid Environment. *Journal of Chinese Society for Corrosion and Protection*, 38(5), 455-462.
[33] Atapour M., Dana M. M. & Ashrafizadeh F. (2015). A corrosion study of grain-refined 304l stainless steels produced by the martensitic process. *International Journal of ISSI*, 12 (2), 30-38.
[34] Saifu D., Shuangbao W., Linyue W., Jianting L. & Yujie W. (2017). Influence of Chloride on Passive Film Chemistry of 304 Stainless Steel in Sulphuric Acid Solution by Glow Discharge Optical Emission Spectrometry Analysis, *Int. J. Electrochem. Sci.*, 12, 1106 –1117.
[35] Wan P., Ma L., Cheng X. & Li X. (2021) Influence of Grain Refinement on the Corrosion Behavior of Metallic Materials: *A Review Int. J. Miner., Metall. Mater.*, 28, 1112-1126,
[36] Sato, N. (2001). The Stability and Breakdown of Passive Oxide Films on Metals. *J. Indian Chem. Soc*., 78, 19–26.

[37] Sutrimo Ating Sudradjat, Rayhan Nugraha Fachari Koeshardono Aris Suryyadi Deni Mulyana & Ita Casmita (2019). Effect of Heat Input Variations to the Mechanical Properties and Pitting Corrosion in Disisimilar Stainless-Steel Welding, *International Journal of Advances in Scientific Research and Engineering (IJASRE)*, 5(10), 116-123.
[38] Pauli L., Jani R., Heikki R. & Teemu S. (2016). Characterisation of Local Grain Size Variation of Welded Structural Steel, *Weld World*, 60, 673–688.
[39] Apurv, C. & Vijaykumar, S. J. (2014). Influence of Heat Input on Mechanical Properties and Microstructure of Austenitic 202 Grade Stainless Steel Weldments. *WSEAS Transactions on Applied and Theoretical Mechanics*, 9, 222-228
[40] Hendrikus Dwijayanto Wibowo Surtargo (2021). Corrosion Rate of Stainless Steel 304 in HNO3 Solution, Arkus, 7(1), https://hmpublisher.com/India.php/arkus.
[41] Olsson, C.O.A. & Landolt, D. (2003). Passive Films on Stainless Steels-Chemistry, Structure and Growth, Electrochimica Acta, 48,(9), 1093- 1104.
[42] Sajay K.G., Avinash R. R., Meghanshu V. & MohdZaharKhad Y. (2019). Effect of Heat Input on Microstructure and Mechanical Properties in Gas Metal Arc Welding of Ferrite Stainless Steel. *Material Research Express*,(3).
[43] Thewlis, C. & Milner, D. R. (1977). Inclusion Formation in Arc Welding, Welding Research Supplement, 281-288.
[44] Prabhu, P. & Rajnish, G. (2016). Effect of Welding Parameters on Pitting Behavior of GTAW of DSS and Super DSS Weldments http://dx.doi.org/10.1016/j.jestch.2016.01.013 a
[45] Abdelfatah A., Raslan A. M. & Mohammed L. Z (2022). Corrosion Characteristics of 304 Stainless Steel in Sodium Chloride and Sulfuric Acid Solutions, *Int. J. Electrochem Sci*.,17(4) , 220417. 15100.
[46] Gigović-Gekić, A., Bikić, F. & Avdušinović, H. (2018). Influence of the Delta Ferrite Content on the Corrosion Behavior of Austenitic Stainless Steel Nitronic 60, Bulletin of the Chemists and Technologists of Bosnia and Herzegovina, 50, 31-34.
[47] Gekić, A., Oruč, M. & Gojić, M. (2011). Determination of the Content of Delta Ferrite in Austenitic Stainless Steel Nitronic 60, In Proceedings of 15th International Research/Expert Conference, Prague, Czech Republic, 157-160.
[48] Subodh, K. & Shahi, A. S. (2011). Effect of Heat Input on the Microstructure and Mechanical Properties of Gas Tungsten Arc Welded AISI 304 Stainless Steel Joints, Materials and Design, 32, 3617–3623.